Inverter Nonlinearity Compensation Through Deadtime Effect Estimation

Joon-Hee Lee, *Student Member, IEEE*, and Seung-Ki Sul, *Fellow, IEEE*

***Abstract*—This article proposes a method to compensate for the nonlinearity of an inverter through the estimation of the deadtime effect. The deadtime effect varies with the manufacturing tolerance of the inverter circuit itself and operating conditions, such as conducting current, dc-link voltage, and temperature. For the accurate compensation of the nonlinearity, the effect of the deadtime should be estimated in realtime. That effect on the control of the inverter is significantly affected by the pulsewidth modulation (PWM) scheme because the deadtime occurs only at the switching instant of the inverter, and the PWM scheme solely decides the switching. The proposed method exploits the difference of voltage error from the deadtime effect according to different PWM schemes. By comparing the effects with two different PWM schemes, namely continuous PWM and discontinuous PWM, the voltage error to a specific inverter caused by the deadtime can be identified. Several experimental tests are carried out to verify the validity of the proposed method. The results reveal that the voltage error due to the deadtime can be identified in the range of 100 mV at 300-V dc link. It is equivalent to 30 ns resolution in deadtime.**

***Index Terms*—Deadtime effect, feedforward control, inverter nonlinearity, pulsewidth modulation (PWM).**

I. Introduction

A DEADTIME refers to an intentional blanking of the gating signals of two switches in an inverter leg to prevent shoot through. Thus, the output voltages of the inverter become different from the voltage references, and it results in the voltage error to the load. Additionally, the ON-state voltage drop of the power semiconductor switches also results in another voltage error. Such voltage errors can be called the inverter nonlinearity effect (INE).

The INE causes the output voltage distortion of the inverter, and the harmonics in output currents increase due to the voltage distortion. Also, the voltage reference of the inverter, which is usually used for control purposes, such as input to the observers of the control loop [1], [2], would be different from the actual output voltage to the load. The difference would degrade the control performance of the motor drive system severely, especially in the case of parameter estimation [3], model-based sensorless drive [4], [5], and the stability of *V/F* control of an induction motor (IM) [6].

To overcome this, there have been lots of research articles dealing with the compensation of the INE. Some attempts intentionally modify the gating signal [7], [8] or the voltage reference for compensation. The modifications were based on the information of the devices given by manufacturers, analytic approach considering parasitic capacitance and snubber capacitance [9], [10], and measured experimentally [11]. Those were implemented through fitting function [12] and lookup table based compensation [13]. However, to guarantee the performance of the compensation on broad operating conditions, it required lots of pretests and memories to store. The others utilized the disturbance observer, which regarded the INE as a disturbance [14]–[16]. It was expected to track the disturbance in a wide operating range. Still, it needs electrical parameters of the system, such as inductance and back electromotive force (EMF) constant of motor, which could vary depending on operating conditions and manufacturing tolerance [14], [15].

Therefore, in this article, an INE compensation method is proposed, which covers broad operating conditions by identifying the variation of deadtime effect online. It is based on the fact that the deadtime effect becomes different depending on the pulsewidth modulation (PWM) schemes. Unlike the other methods, it does not require any electrical parameter, such as inductance and back EMF constant, but tracks the variation of deadtime effect in a wide range of current operating points during the drive system operation. Also, the analytic study of the deadtime effect with different PWM schemes is introduced to improve the performance of the proposed compensation. The validity of the proposed method is verified by the experimental test.

In addition to the previously presented work [17], this article provides the following.

1) A feedforward-based deadtime effect identification method to improve dynamic performance.
2) The experimental result with different inverters and IMs in various operating conditions.

II. INE With Different PWM Schemes

A voltage error δv_{xn} due to the INE in a leg in Fig. 1 can be defined as (1), where $v_{xn}{}^{*}$ stands for the *x*-phase pole

Manuscript received September 10, 2020; revised December 19, 2020; accepted February 6, 2021. Date of publication February 23, 2021; date of current version June 1, 2021. This work was supported by the Seoul National University Electric Power Research Institute of the Korea Institute of Energy Technology Evaluation, and in part by Planning, and in part by the Brain Korea 21 Plus Project in 2020 funded by the Ministry of Trade, Industry, and Energy, Republic of Korea. Recommended for publication by Associate Editor B. Mirafzal. *(Corresponding author: Seung-Ki Sul.)*

The authors are with the Department of Electrical and Computer Engineering, Seoul National University, Seoul 151-744, South Korea (e-mail: joonhee.lee@eepel.snu.ac.kr; sulsk@plaza.snu.ac.kr).

Color versions of one or more of the figures in this article are available online at https://doi.org/10.1109/TPEL.2021.3061285.

Digital Object Identifier 10.1109/TPEL.2021.3061285

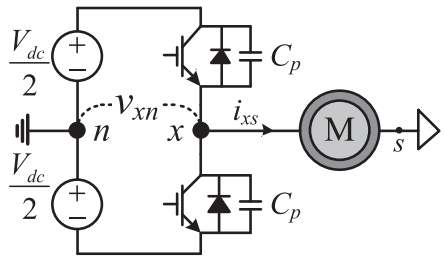

Fig. 1. One leg of an inverter.

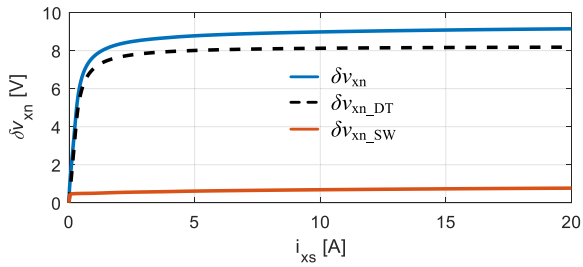

Fig. 2. Voltage error from inverter nonlinearity.

TABLE I
PARAMETERS OF TARGET INVERTER

Parameter	Value
V_{DC}	300 V
f_{sw}	10 kHz
T_d	3 μs
Switches	
Infineon FS50R12KT4_B15	

voltage reference and v_{xn} for the actual output voltage. Here, the subscript x means a specific phase among three phases of the inverter

$$\delta v_{xn} \triangleq v_{xn}^* - v_{xn}. \tag{1}$$

Fig. 2 shows δv_{xn} according to the phase current i_{xs} based on the parameters in Table I. δv_{xn} can be divided into two components, namely δv_{xn_SW} and δv_{xn_DT}. δv_{xn_SW} comes from the ON-state voltage of the switches and δv_{xn_DT} from the deadtime effect considering parasitic capacitances C_p of the leg. Especially, δv_{xn_DT} according to i_{xs} can be expressed as

$$\delta v_{xn\_DT}(i_{xs}) = \begin{cases} -\frac{1}{2}\frac{C_o {V_{DC}}^2}{T_{sw}}\frac{1}{i_{xs}} - \frac{T_d}{T_{sw}}V_{DC}, & (i_{xs} < -I_c) \\ \frac{{T_d}^2}{2C_o T_{sw}} i_{xs}, & (-I_c \le i_{xs} < I_c) \\ -\frac{1}{2}\frac{C_o {V_{DC}}^2}{T_{sw}}\frac{1}{i_{xs}} + \frac{T_d}{T_{sw}}V_{DC}, & (I_c \le i_{xs}) \end{cases} \tag{2}$$

which can be derived by the average volt-sec loss and gain during deadtime in one switching period. Here, $C_o = 2C_p$, the critical current $I_c = C_o \cdot V_{DC}/T_d$, and T_{sw} is the switching period.

Meanwhile, the two components are different in the respect that δv_{xn_SW} exists because of the conducting current, i_{xs}, in the phase, while δv_{xn_DT} does only on the phase switched ON and OFF

$$v_{xn}^* = v_{xs}^* + v_{sn}^*. \tag{3}$$

The switching of each phase depends on the pole voltage reference, ${v_{xn}}^*$ in (3), which is determined by a phase voltage reference ${v_{xs}}^*$ and an offset voltage ${v_{sn}}^*$. Since ${v_{sn}}^*$ varies according to different PWM schemes, ${v_{xn}}^*$ and, thus, the switching of each phase become different even with the same ${v_{xs}}^*$. Fig. 3 shows ${v_{an}}^*$, δv_{an}, δv_{an_SW}, and δv_{an_DT} with different PWM schemes when ${v_{as}}^*$ and i_{as} are the same. Continuous PWM (CPWM) is applied in Fig. 3(a) and 60° discontinuous PWM (DPWM) on Fig. 3(b). Here, CPWM refers that v_{sn}^* is set as (4) and DPWM is as (5). $v_{\max}^*$ and $v_{\min}^*$ mean the maximum and minimum phase voltage reference among three phases

$$v_{sn}^* = -(v_{\max}^* + v_{\min}^*)/2 \tag{4}$$

$$v_{sn}^* = \begin{cases} V_{dc}/2 - v_{\max}^* & (v_{\max}^* + v_{\min}^*) \ge 0 \\ -V_{dc}/2 - v_{\min}^* & (v_{\max}^* + v_{\min}^*) < 0. \end{cases} \tag{5}$$

In Fig. 3, δv_{an_SW} exists for the entire period regardless of PWM schemes because it is only determined by i_{as}. However, in the case of δv_{an_DT}, it is affected by ${v_{an}}^*$ as well as i_{as} because the switching does not occur in the clamped phase in DPWM. Thus, δv_{an_DT} appears for the whole period with CPWM, while it becomes zero with DPWM when ${v_{an}}^*$ is clamped to $V_{DC}/2$ or $-V_{DC}/2$.

The conceptual circuit diagram of the motor drive system is described, as shown in Fig. 4. The motor is simplified as resistance R_s, phase inductances L_{xs}, and back EMF E_{xs}. The inverter is expressed as voltage sources δv_{xn_SW} and δv_{xn_DT} in each phase. It is noted that δv_{xn_DT} is a variable voltage source depending on the PWM scheme.

III. Proposed INE Compensation Method I With Tracking Variation of Deadtime Effect–Feedback Method

In the voltage error caused by INE, the error by the deadtime effect usually takes a larger portion than that by the ON-state voltage drop. The error by the deadtime effect varies with operating conditions, such as dc-link voltage, current at the switching instant, device tolerance, including gating circuit, and temperatures [18]. Thus, to ensure the reasonable performance of the compensation of INE, the variation of deadtime effect should be identified online. The effective deadtime is affected not only by the preset deadtime but also by the turn-ON/OFF delay of the device and gate drive circuit, which highly depends on the device temperature. In other words, the effective deadtime $T_{d,\text{eff}}$ expressed as $T_d + T_{on} - T_{off}$ would vary due to several unpredictable reasons. Considering the effective deadtime, T_d in (2) can be replaced as $T_{d,\text{eff}}$.

Fig. 5 shows the current control block diagram of an IM drive system containing the proposed INE compensation and ${v_{sn}}^*$ calculation part. In this diagram, the INE of the PWM inverter is modeled as a disturbance voltage term, $\delta \mathbf{v_{abc}}$, which consists of $\delta \mathbf{v_{abcn\_SW}}$ and $\delta \mathbf{v_{abcn\_DT}}$, as shown in Fig. 4.

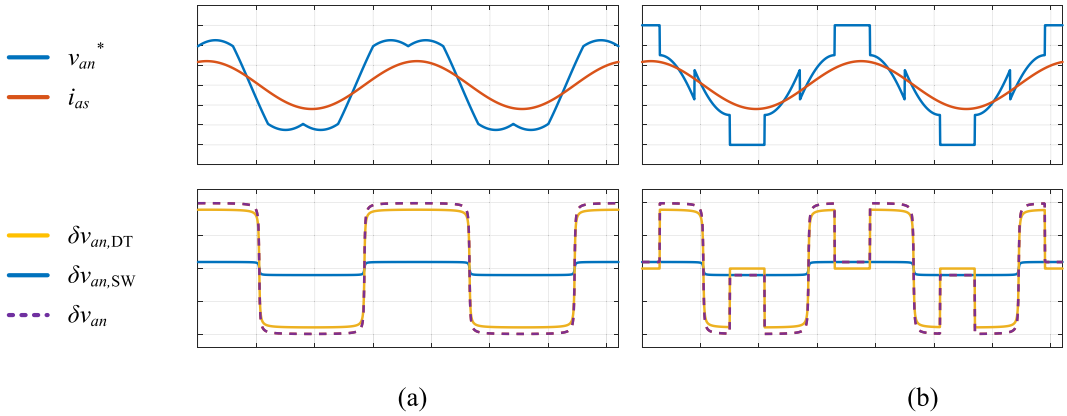

Fig. 3. Pole voltage, phase current, and voltage error. (a) CPWM. (b) 60° DPWM.

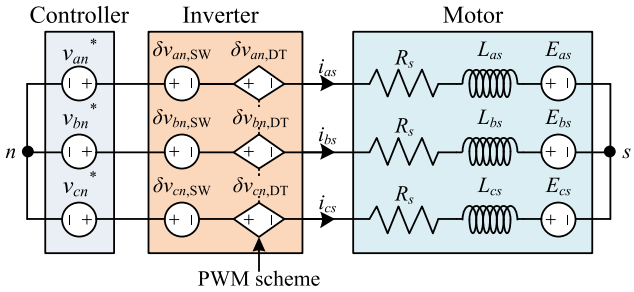

Fig. 4. Conceptual circuit diagram of controller–inverter–motor drive system.

To compensate INE, in the proposed part, the phase voltage reference $\mathbf{v_{abcs}}^*$ is converted intentionally to pole voltage reference $\mathbf{v_{abcn}}^{**}$ according to CPWM and DPWM. As aforementioned in Section II, $\delta\mathbf{v_{abcn\_SW}}$ exists on all phases conducting current, while $\delta\mathbf{v_{abcn\_DT}}$ does only on the phase switched ON/OFF. Thus, the proposed method in Fig. 6 separates the compensation of each part into before/after v_{sn}^* calculation. At first, the compensations of $\delta\mathbf{v_{abc\_SW}}$ are added on all $\mathbf{v_{abcs}}^*$, and $\mathbf{v_{abcn}}^*$ is determined with v_{sn}^* calculation. Then, the compensation of $\delta\mathbf{v_{abc\_DT}}$ is added on $\mathbf{v_{abcn}}^*$ except the clamped phase of DPWM to generate the final pole voltage reference $\mathbf{v_{abcn}}^{**}$. Thus, the proposed method can compensate for the INE regardless of PWM schemes.

To track the variation of the deadtime effect, $\delta\hat{\mathbf{v}}_{\mathbf{abc,DT}}$ is adjusted online, while $\delta\hat{\mathbf{v}}_{\mathbf{abc,SW}}$ is set as a fixed function. For a simple implementation, $\delta\hat{\mathbf{v}}_{\mathbf{abc,SW}}$ and $\delta\hat{\mathbf{v}}_{\mathbf{abc,DT}}$ are modeled as

$$\begin{aligned}\delta\hat{v}_{xn\_\mathrm{SW}} &= \hat{V}_{\mathrm{sat,SW}} \cdot \mathrm{sign}(i_{xs}) \\ \delta\hat{v}_{xn\_\mathrm{DT}} &= 2/\pi \cdot \hat{V}_{\mathrm{sat,DT}} \cdot a\tan(\hat{K}_{\mathrm{DT}} i_{xs})\end{aligned} \tag{6}$$

where the variables with "^" mean the estimated value. In (6), $\hat{V}_{\mathrm{sat,SW}}$ can be determined from the device datasheet, and it is fixed as a constant value, even though it also varies according to the device temperature. And, $\hat{K}_{\mathrm{DT}}$ can be set by a simple experimental test. Since $\hat{K}_{\mathrm{DT}}$ is highly affected by the output parasitic capacitance of the inverter, which does not vary with temperature, it can be set as a fixed value too.

Meanwhile, if the deadtime effect is not compensated correctly, the current controller adjusts $\mathbf{v}_{\mathbf{dqs}}^{\mathbf{e}*}$ to cancel out the disturbance. To elaborate this, it is assumed that there is no compensation of INE. Then, the voltage output of the current controller $\mathbf{v}_{\mathbf{dqs}}^{\mathbf{e}*}$ can be expressed as

$$\mathbf{v}_{\mathbf{dqs}}^{\mathbf{e}*} = \mathbf{v}_{\mathbf{dqs,MOT}}^{\mathbf{e}*} + \delta\mathbf{v}_{\mathbf{dqs,SW}}^{\mathbf{e}} + \delta\mathbf{v}_{\mathbf{dqs,DT}}^{\mathbf{e}}. \tag{7}$$

$\mathbf{v}_{\mathbf{dqs}}^{\mathbf{e}*}$ has three components, $\mathbf{v}_{\mathbf{dqs,MOT}}^{\mathbf{e}*}$, $\delta\mathbf{v}_{\mathbf{dqs,SW}}^{\mathbf{e}}$, and $\delta\mathbf{v}_{\mathbf{dqs,DT}}^{\mathbf{e}}$. Based on Fig. 4, $\mathbf{v}_{\mathbf{dqs,MOT}}^{\mathbf{e}*}$ represents the component to regulate the current in the motor. The $\delta\mathbf{v}_{\mathbf{dqs,SW}}^{\mathbf{e}}$ and $\delta\mathbf{v}_{\mathbf{dqs,DT}}^{\mathbf{e}}$ represent the components to reject the disturbance caused by the ON-state voltage drop and the deadtime effect. Since the current control is operated in a closed-loop manner, $\mathbf{v}_{\mathbf{dqs}}^{\mathbf{e}*}$ should be adjusted to (7) in order to regulate the current as desired. And, it is noted that the amount of adjustment in $\mathbf{v}_{\mathbf{dqs}}^{\mathbf{e}*}$ would be different with different PWM schemes because $\delta\mathbf{v}_{\mathbf{dqs,DT}}^{\mathbf{e}}$ itself is different in the case of CPWM and DPWM. The principle of online tracking of the deadtime effect is based on this difference.

Fig. 7(c) shows the conceptual diagram of the operation of the estimator, which assumes that $T_{d,\mathrm{eff}}$ increases from its initial value due to the variation of the operating conditions. Thus, the magnitude of $\delta\mathbf{v_{abc,DT}}$ also increases because the magnitude of $\delta v_{xn\_\mathrm{DT}}$ in (2) is highly related to $T_{d,\mathrm{eff}}$. To detect the variation of $\delta\mathbf{v_{abc,DT}}$, the proposed method alternates the PWM scheme between CPWM and 60° DPWM, while the speed and current reference are fixed. Then, the output voltages from the current controller, v_{ds}^{e*} and v_{qs}^{e*}, increase in CPWM and decrease in DPWM because $\delta\mathbf{v}_{\mathbf{dqs,DT}}^{\mathbf{e}}$ with CPWM is larger than that with DPWM. To ignore the influence of harmonics in output voltages and to take the variation of dc component, low-pass filters (LPF) are applied to $\mathbf{v}_{\mathbf{dqs}}^{\mathbf{e}*}$. The cutoff frequency ω_c is designed as (8) to attenuate the sixth harmonics in the output voltages. Also, the duration of each PWM T_{PWM} is set considering the settling time of LPF as (9)

$$\omega_c = \frac{6\omega_e}{10} \tag{8}$$

$$T_{\mathrm{PWM}} = \frac{5}{\omega_c}. \tag{9}$$

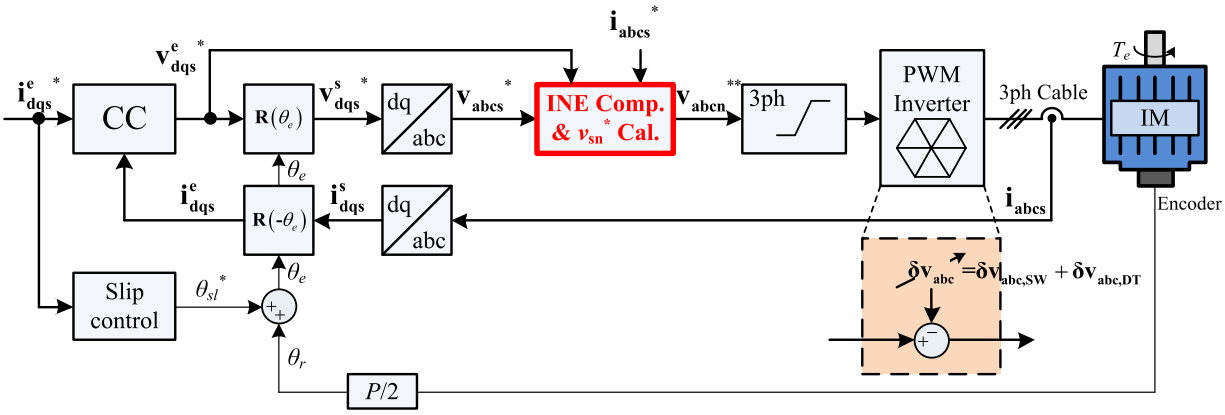

Fig. 5. Current control block diagram in an IM drive system.

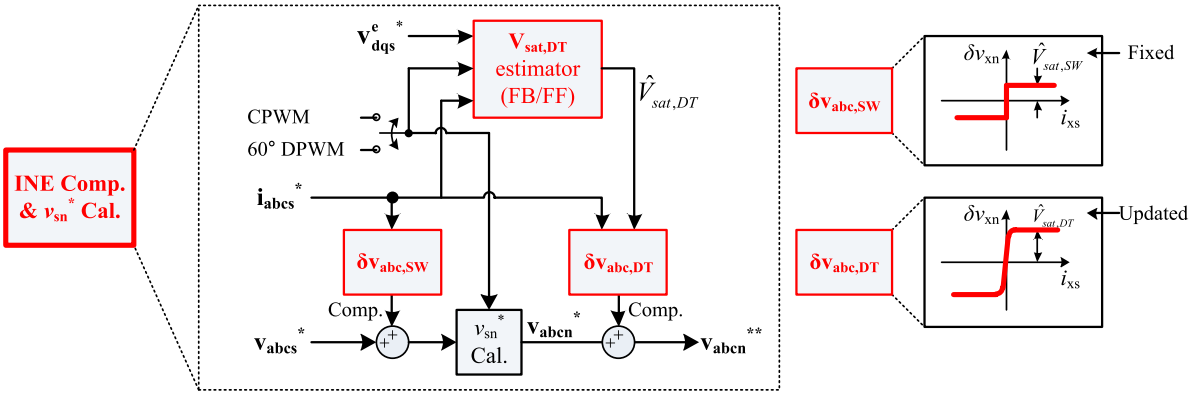

Fig. 6. Proposed inverter nonlinearity compensation and v_{sn}^* calculation block.

After one alternation of the PWM scheme, the proportional-integral (PI) controller is triggered, and it takes Δv_{PWM} as an error to update $\hat{V}_{\mathrm{sat,DT}}$ value. Δv_{PWM} is defined as

$$\Delta v_{\mathrm{PWM}} = (v_{d,\mathrm{CP}} + v_{q,\mathrm{CP}}) - (v_{d,\mathrm{DP}} + v_{q,\mathrm{DP}}) \tag{10}$$

where $v_{d,\mathrm{CP}}$, $v_{q,\mathrm{CP}}$, $v_{d,\mathrm{DP}}$, and $v_{q,\mathrm{DP}}$ are the sampled values at the end of each PWM scheme, as shown in Fig. 7(c)

As $\hat{V}_{\mathrm{sat,DT}}$ reaches the actual value, the filtered value of $\mathbf{v}_{\mathbf{dqs}}^{\mathbf{e}*}$ becomes the same regardless of PWM schemes because the INE is correctly compensated with the proposed method.

IV. Proposed INE Compensation Method II With Tracking Variation of Deadtime Effect–Feedforward Method

Generally, the dynamic performance of the estimator, both with feedforward and feedback methods, can be significantly improved compared with that of the estimator only with the feedback method. Thus, in this section, a novel calculation method of the feedforward term, $\hat{V}_{\mathrm{sat,DT,FF}}$, in Fig. 7(a) is proposed.

A. Fundamental Component Calculation of $\delta\hat{v}_{xn\_\mathrm{DT}}$

The proposed feedback-based estimation method in Section III is based on Δv_{PWM} in (10). Since Δv_{PWM} utilizes the filtered signals of $\mathbf{v}_{\mathbf{dqs}}^{\mathbf{e}*}$, Δv_{PWM} is highly related to the fundamental component of $\delta\hat{v}_{xn\_\mathrm{DT}}$, which changes with i_{xs} and PWM methods. In other words, Δv_{PWM} can be directly calculated if a fundamental component of $\delta\hat{v}_{xn\_\mathrm{DT}}$ is known.

Fig. 8 shows v_{an}^*, i_{as}, and $\delta v_{an\_\mathrm{DT}}$ of CPWM and DPWM with various current angles ϕ_i. When v_{xn}^* is aligned to $\omega t = 0°$ and i_{xs} is set as $I_m\cos(\omega t+\phi_i)$, $\delta\hat{v}_{xn\_\mathrm{DT}}$ with CPWM is expressed as

$$\delta\hat{v}_{xn\_\mathrm{DT,CP}}(\omega t) = \frac{2\hat{V}_{\mathrm{sat,DT}}}{\pi}\mathrm{atan}\left(K^*\cos(\omega t+\phi_i)\right) \tag{11}$$

where $K^* = \hat{K}_{\mathrm{DT}} I_m$. Then, the fundamental component of $\delta\hat{v}_{xn\_\mathrm{DT,CP}}$ in phase of i_{xs}, $\delta\hat{v}_{xn\,,\mathrm{CP,Fund}}$, is calculated with

$$\begin{aligned}
&\delta\hat{v}_{xn\,,\mathrm{CP,Fund}} \\
&= \frac{1}{\pi}\int_{\omega t=-\pi}^{\omega t=\pi} \delta\hat{v}_{xn_\mathrm{DT,CP}}(\omega t)\cdot\cos(\omega t+\phi_i)d(\omega t) \\
&= \hat{V}_{\mathrm{sat,DT}}\cdot\frac{8}{\pi^2}\cdot f\left(K^*,\frac{\pi}{2}\right)
\end{aligned} \tag{12}$$

where $f(K^*,\omega t)$ is defined as

$$f(K^*,\omega t) = \int\{\mathrm{atan}\left(K^*\cos(\omega t)\right)\cos(\omega t)\}d(\omega t)$$

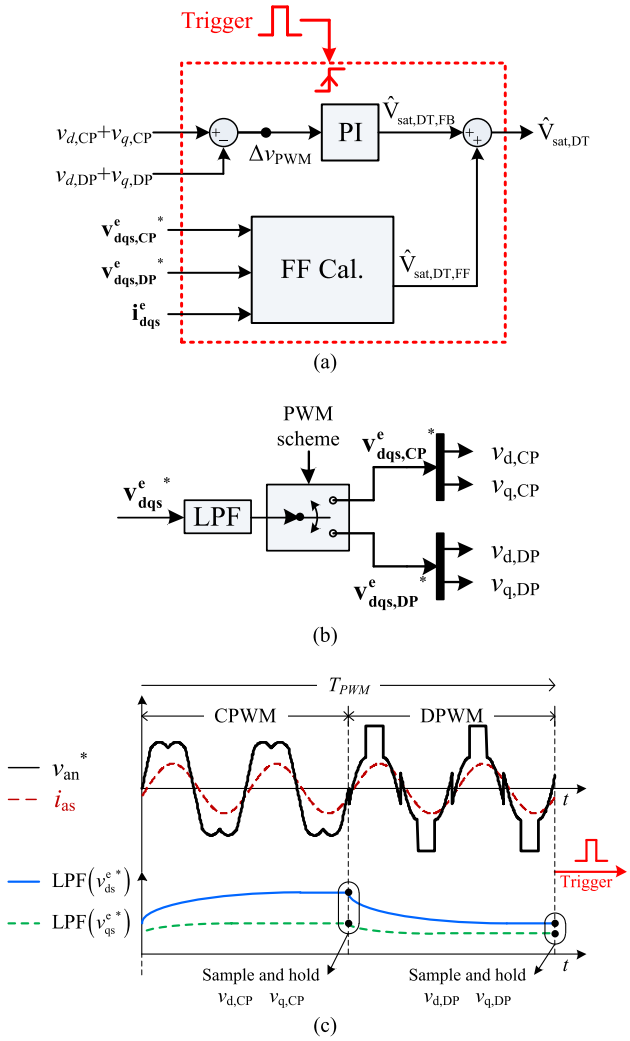

Fig. 7. $V_{\mathrm{sat,DT}}$ estimator. (a) Block diagram. (b) Filtering process. (c) Conceptual waveforms of signals in the block diagram.

$$= -\frac{1}{K^*}\left\{\begin{array}{l} -\sqrt{K^{*2}+1}\,\mathrm{atan}\left(K^* - \sqrt{K^{*2}+1}\tan\frac{\omega t}{2}\right) \\ +\sqrt{K^{*2}+1}\,\mathrm{atan}\left(K^* + \sqrt{K^{*2}+1}\tan\frac{\omega t}{2}\right) \\ +K^*\sin\omega t\cdot\mathrm{atan}\left(K^*\cos\omega t\right) - \omega t \end{array}\right\}. \tag{13}$$

Meanwhile, $\delta\hat{v}_{xn\_\mathrm{DT}}$ with DPWM is expressed as

$$\delta\hat{v}_{xn\_\mathrm{DT,DP}}(\omega t) = \begin{cases} 0 & -\frac{\pi}{6} \le \omega t < \frac{\pi}{6} \\ \frac{2\hat{V}_{\mathrm{sat,DT}}}{\pi}\mathrm{atan}\left(K^*\cos(\omega t+\phi_i)\right) & \text{otherwise.} \end{cases} \tag{14}$$

Then, the fundamental component of $\delta\hat{v}_{xn\_\mathrm{DT,DP}}$ in phase of i_{xs}, $\delta\hat{v}_{xn,\mathrm{DP,Fund}}(\phi_i)$, is

$$\begin{aligned} &\delta\hat{v}_{xn,\mathrm{DP,Fund}}(\phi_i) \\ &= \frac{1}{\pi}\int_{-\pi}^{\pi}\delta\hat{v}_{xn\_\mathrm{DT,DP}}(\omega t)\cdot\cos(\omega t+\phi_i)d(\omega t) \\ &= \hat{V}_{\mathrm{sat,DT}}\cdot\frac{4}{\pi^2}\cdot g(K^*,\phi_i) \end{aligned} \tag{15}$$

where $g(K^*,\phi_i)$ is defined as

$$g(K^*,\phi_i) = \begin{cases} f\left(K^*,\phi_i+\frac{\pi}{6}\right) - f\left(K^*,\phi_i+\frac{5\pi}{6}\right) & \left(-\frac{\pi}{2} \le \phi_i < -\frac{\pi}{3}\right) \\ f\left(K^*,\frac{\pi}{2}\right) - f\left(K^*,-\frac{\pi}{2}\right) & \left(-\frac{\pi}{3} \le \phi_i < \frac{\pi}{3}\right) \\ -f\left(K^*,\phi_i+\frac{\pi}{6}\right) + f\left(K^*,\phi_i-\frac{\pi}{6}\right) & \left(-\frac{\pi}{3} \le \phi_i < \frac{\pi}{3}\right) \\ f\left(K^*,\phi_i-\frac{\pi}{6}\right) - f\left(K^*,\phi_i-\frac{5\pi}{6}\right) & \left(\frac{\pi}{3} \le \phi_i \le \frac{\pi}{2}\right). \end{cases} \tag{16}$$

It is noted that $\delta\hat{v}_{xn,\mathrm{CP,Fund}}$ is constant regardless of current angle ϕ_i, while $\delta\hat{v}_{xn,\mathrm{DP,Fund}}(\phi_i)$ is a function of ϕ_i because $\delta\hat{v}_{xn\_\mathrm{DT}}$ with DPWM is clamped to zero when ωt is within $(-\pi/3, \pi/3)$.

To calculate Δv_{PWM}, $\delta\hat{\mathbf{v}}_{\mathbf{abcn,x,Fund}}(\mathbf{x} = \text{CP or DP})$ is converted to $\delta\hat{\mathbf{v}}^{\mathbf{i}}_{\mathbf{dqs,x,Fund}}(\phi_i)$ as

$$\begin{aligned} \delta\hat{\mathbf{v}}^{\mathbf{i}}_{\mathbf{dqs,x,Fund}}(\phi_i) &= \mathbf{R}(-\phi_i)\mathbf{T}_{\alpha\beta}\begin{bmatrix}\delta\hat{v}^i_{an,x,\mathrm{Fund}} \\ \delta\hat{v}^i_{bn,x,\mathrm{Fund}} \\ \delta\hat{v}^i_{cn,x,\mathrm{Fund}}\end{bmatrix} \\ &= \begin{bmatrix}\cos\phi_i & \sin\phi_i \\ -\sin\phi_i & \cos\phi_i\end{bmatrix}\begin{bmatrix}\frac{2}{3} & -\frac{1}{3} & -\frac{1}{3} \\ 0 & \frac{1}{\sqrt{3}} & -\frac{1}{\sqrt{3}}\end{bmatrix}\begin{bmatrix}\delta\hat{v}^i_{an,x,\mathrm{Fund}} \\ \delta\hat{v}^i_{bn,x,\mathrm{Fund}} \\ \delta\hat{v}^i_{cn,x,\mathrm{Fund}}\end{bmatrix} \end{aligned} \tag{17}$$

where superscript i means the reference frame aligned to ϕ_i. Also, $\mathbf{R}$ and $\mathbf{T}_{\alpha\beta}$ stand for the rotating and Clarke transformation matrix, respectively. Fig. 9 shows the magnitude and phase of $\delta\hat{\mathbf{v}}^{\mathbf{i}}_{\mathbf{dqs,CP,Fund}}(\phi_i)$ and $\delta\hat{\mathbf{v}}^{\mathbf{i}}_{\mathbf{dqs,DP,Fund}}(\phi_i)$ based on the parameters in Table I. The magnitude of $\delta\hat{\mathbf{v}}^{\mathbf{i}}_{\mathbf{dqs,CP,Fund}}(\phi_i)$ is the same irrespective of ϕ_i and the phase is zero. That is, the deadtime effect in the case of CPWM can be modeled as an equivalent resistance [19], [20]

$$R_{\mathrm{eq,CP}} = \frac{\left|\delta\hat{\mathbf{v}}^{\mathbf{i}}_{\mathbf{dqs,CP,Fund}}\right|}{\left|\mathbf{i}^{\mathbf{i}}_{\mathbf{dqs}}\right|} = \frac{\delta\hat{v}^i_{ds,\mathrm{CP,Fund}}}{i^i_{ds}}. \tag{18}$$

However, the magnitude and phase of $\delta\hat{\mathbf{v}}^{\mathbf{i}}_{\mathbf{dqs,DP,Fund}}(\phi_i)$ vary with ϕ_i, so the deadtime effect with DPWM is not modeled only as a resistance but as a sum of resistance and reactance, such as

$$R_{\mathrm{eq,DP}} = \frac{\delta\hat{v}^i_{ds,\mathrm{DP,Fund}}}{i^i_{ds}}, \quad X_{\mathrm{eq,DP}} = \frac{\delta\hat{v}^i_{qs,\mathrm{DP,Fund}}}{i^i_{ds}}. \tag{19}$$

B. Feedforward Term Calculation

Based on the equivalent impedance from the deadtime effect, the feedforward term $\hat{V}_{\mathrm{sat,DT,FF}}$ can be derived. For derivation, it is assumed that no INE compensation is applied in the current control of IM. Adopting the equivalent impedance of the deadtime effect, (7) in the case of CPWM is expressed as

$$\mathbf{v}^{\mathbf{e}*}_{\mathbf{dqs,CP}} = \mathbf{v}^{\mathbf{e}*}_{\mathbf{dqs,MOT}} + \delta\mathbf{v}^{\mathbf{e}}_{\mathbf{dqs,SW}} + R_{\mathrm{eq,CP}}\mathbf{i}^{\mathbf{e}}_{\mathbf{dqs}} \tag{20}$$

and that in case of DPWM as

$$\begin{aligned} \mathbf{v}^{\mathbf{e}*}_{\mathbf{dqs,DP}} = \mathbf{v}^{\mathbf{e}*}_{\mathbf{dqs,MOT}} + \delta\mathbf{v}^{\mathbf{e}}_{\mathbf{dqs,SW}} \\ + (R_{\mathrm{eq,DP}} + jX_{\mathrm{eq,DP}})\mathbf{i}^{\mathbf{e}}_{\mathbf{dqs}}. \end{aligned} \tag{21}$$

Since $(\mathbf{v}^{\mathbf{e}*}_{\mathbf{dqs,MOT}} + \delta\mathbf{v}^{\mathbf{e}}_{\mathbf{dqs,SW}})$ term is the same for both CPWM and DPWM, subtracting (21) from (20) and dot product

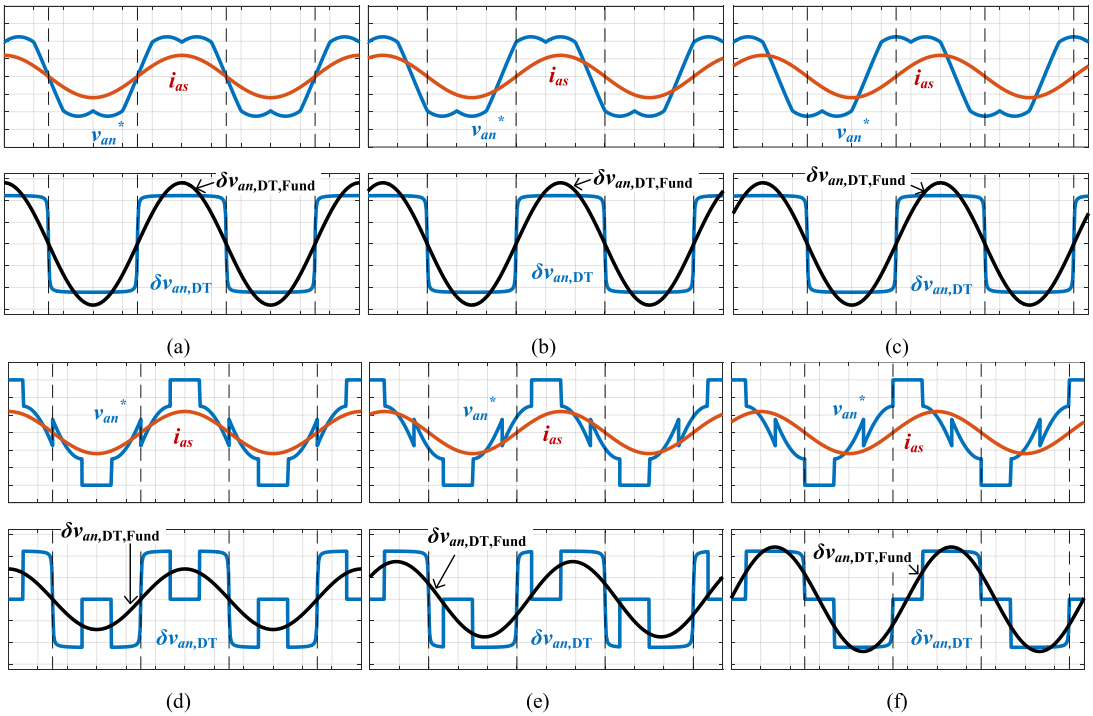

Fig. 8. $v_{an}{}^*$, i_{as}, and $\delta v_{an,\mathrm{DT}}$ according to PWM method and current angle ϕ_i. (a) CPWM, $\phi_i = 0°$. (b) CPWM, $\phi_i = 30°$. (c) CPWM, $\phi_i = 60°$. (d) DPWM, $\phi_i = 0°$. (e) DPWM, $\phi_i = 30°$. (f) DPWM, $\phi_i = 60°$.

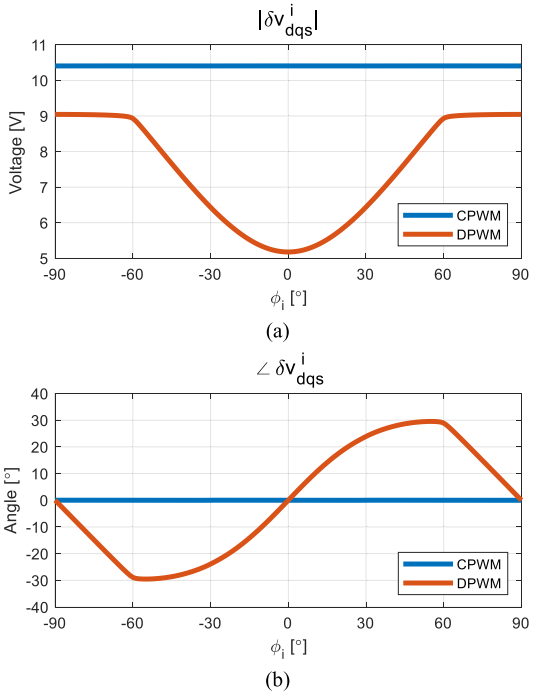

Fig. 9. $\delta\hat{\mathbf{v}}^{\mathbf{i}}_{\mathbf{dqs,CP,Fund}}(\phi_i)$ and $\delta\hat{\mathbf{v}}^{\mathbf{i}}_{\mathbf{dqs,DP,Fund}}(\phi_i)$. (a) Magnitude. (b) Phase.

with unit current vector results in

$$\frac{\mathbf{v}^{\mathbf{e*}}_{\mathbf{dqs,CP}} \cdot \mathbf{i}^{\mathbf{e}}_{\mathbf{dqs}}}{\left|\mathbf{i}^{\mathbf{e}}_{\mathbf{dqs}}\right|} - \frac{\mathbf{v}^{\mathbf{e*}}_{\mathbf{dqs,DP}} \cdot \mathbf{i}^{\mathbf{e}}_{\mathbf{dqs}}}{\left|\mathbf{i}^{\mathbf{e}}_{\mathbf{dqs}}\right|}$$

$$= R_{\mathrm{eq,CP}}\left|\mathbf{i}^{\mathbf{e}}_{\mathbf{dqs}}\right| - R_{\mathrm{eq,DP}}\left|\mathbf{i}^{\mathbf{e}}_{\mathbf{dqs}}\right|$$
$$= \delta\hat{v}_{xn\,,\mathrm{CP,Fund}} - \delta\hat{v}_{xn\,,\mathrm{DP,Fund}}(\phi_i). \tag{22}$$

Then, $\hat{V}_{\mathrm{sat,DT,FF}}$ can be achieved by substituting (12) and (15) into (22) as

$$\hat{V}_{\mathrm{sat,DT,FF}} = \frac{\frac{\mathbf{v}^{\mathbf{e*}}_{\mathbf{dqs,CP}} \cdot \mathbf{i}^{\mathbf{e}}_{\mathbf{dqs}}}{\left|\mathbf{i}^{\mathbf{e}}_{\mathbf{dqs}}\right|} - \frac{\mathbf{v}^{\mathbf{e*}}_{\mathbf{dqs,DP}} \cdot \mathbf{i}^{\mathbf{e}}_{\mathbf{dqs}}}{\left|\mathbf{i}^{\mathbf{e}}_{\mathbf{dqs}}\right|}}{\frac{4}{\pi^2}\left(2f(K^*, \pi/2) - g(K^*, \phi_i)\right)} \tag{23}$$

where ϕ_i is achieved as

$$\mathbf{v}^{\mathbf{i*}}_{\mathbf{dqs,DP}} = R(-\theta_i)\mathbf{v}^{\mathbf{e*}}_{\mathbf{dqs,DP}}, \quad \theta_i = a\tan2(i^e_{qs}, i^e_{ds})$$
$$\phi_i = a\tan2(v^{i*}_{qs,\mathrm{DP}}, v^{i*}_{ds,\mathrm{DP}}). \tag{24}$$

By adding $\hat{V}_{\mathrm{sat,DT,FF}}$ on the output of the proposed estimation, the dynamic response can be improved.

V. Experimental Results

To verify the effectiveness of the proposed compensation method, an experimental setup is prepared based on 3.7-kW IM drive system, as shown in Fig. 10. The parameters of the inverter are listed in Table I, and those of IM are in Table II. For a gate driver, TI ISO5852s is used.

First of all, a pretest is conducted to investigate the INE when T_d is set as 3 μs in normal condition, as shown in Fig. 11(a). $\hat{V}_{\mathrm{sat,SW}}$ is set to 1 V according to the datasheet of the switching device. Also, $\hat{V}_{\mathrm{sat,DT}}$ and $\hat{K}_{\mathrm{DT}}$ are set to 8.3 V and 2.7, respectively, which are well fitted to measure δv_{xn}. Meanwhile, according to the datasheet of gate driver [21], $T_{d,\mathrm{eff}}$ would vary up to ± 0.3 μs depending on operating conditions. Thus, to

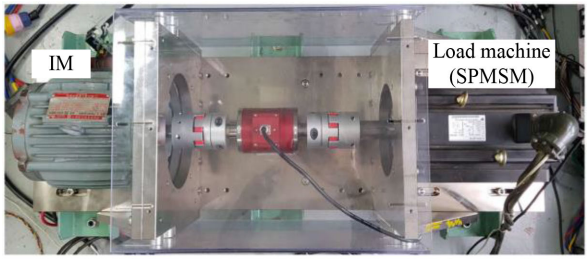

(a)

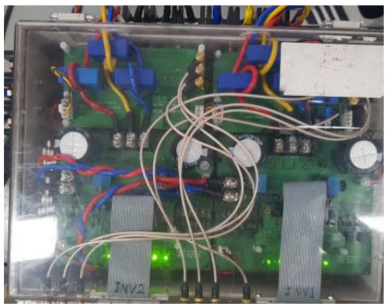

(b)

Fig. 10. Experimental setup. (a) M-G set. (b) Inverter.

TABLE II
PARAMETERS OF IM

Parameter	Value
Rated voltage	220 V_{rms}
Rated current	13.8 A_{rms}
Number of pole	4
R_s	0.5 Ω
L_m	60 mH
L_{ls} ,L_{lr}	6 mH

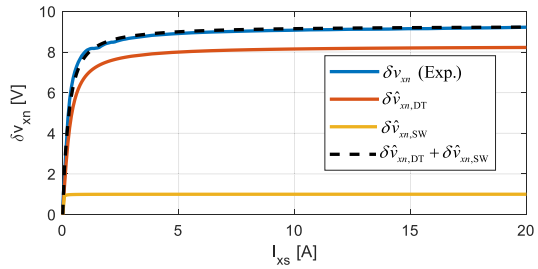

(a)

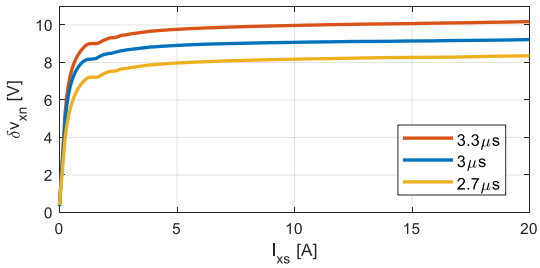

(b)

Fig. 11. Measured δv_{xn} according to i_{xs}. (a) Measured δv_{xn} and the fitting function. (b) Measured δv_{xn} with various $T_d{}^*$.

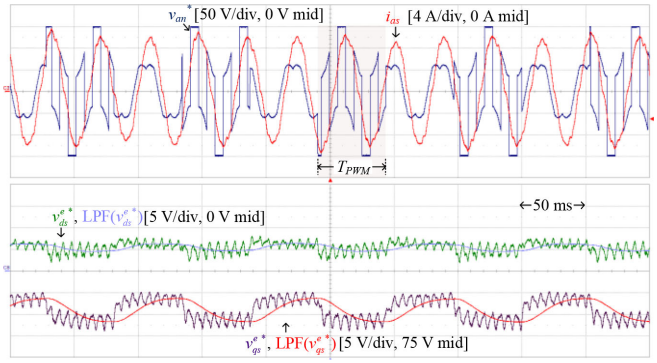

Fig. 12. First experimental result: $\mathbf{v}^{\mathbf{e}*}_{\mathbf{dqs}}$ variation with CPWM and DPWM.

confirm the accuracy of the proposed method, δv_{xn}, according to i_{xs}, is measured again at $T_d{}^* = 3.3$ and 2.7 μs, as shown in Fig. 11(b). It reveals that the voltage error varies by 0.9 V with 0.3 μs of $T_{d,\text{eff}}$ variation.

Fig. 12 shows the first experimental result when the PWM scheme alternates between CPWM and 60° DPWM without the INE compensation. i^e_{ds} and i^e_{qs} are regulated as rated values, 6 and 8 A, respectively. The speed is set as 750 r/min by the load machine. As shown in the first trace, the a-phase pole voltage reference, $v_{an}{}^*$, alternates in the period of T_{PWM} between CPWM and DPWM. With (8) and (9), ω_c and T_{PWM} are set as $2\pi\times15$ rad/s and 53.1 ms, respectively. As shown in the second trace, the current controller adjusts $\mathbf{v}^{\mathbf{e}*}_{\mathbf{dqs}}$ to cancel out the disturbance caused by the INE. Similar to Fig. 7(c), the average value of v^{e*}_{ds} and v^{e*}_{qs} increases when the PWM scheme changes from DPWM to CPWM because a fundamental component of $\delta\mathbf{v}_{\mathbf{abc}}$ with CPWM is larger than that with DPWM.

The second experiment is conducted to verify the performance of the proposed feedback-based $\hat{V}_{\text{sat,DT}}$ identification when the initial value of $\hat{V}_{\text{sat,DT}}$ is set to zero, as shown in Fig. 13. After the proposed method is activated, the PWM scheme is altered between CPWM and DPWM, so the filtered values of v^{e*}_{ds} and v^{e*}_{qs} are fluctuating in the fourth trace. Based on that, $\hat{V}_{\text{sat,DT}}$ is updated and converges to 8.3 V within 2.8 s in the second trace. The third trace shows the $\delta\hat{v}_{an,\text{SW}}$ and $\delta\hat{v}_{an,\text{DT}}$. By estimating $\hat{V}_{\text{sat,DT}}$, $\delta\hat{v}_{an,\text{DT}}$ increases to compensate the deadtime effect, while $\delta\hat{v}_{an,\text{SW}}$ is kept as the initial value. Fig. 14 shows the magnified view of Fig. 13 for the specified regions. As shown in Zoom-in II, $\delta\hat{v}_{an,\text{SW}}$ is always applied even in DPWM, while $\delta\hat{v}_{an,\text{DT}}$ is only applied for the unclamped interval. The Zoom-in III and IV show the current (i^e_{ds}, i^e_{qs}) before and after the proposed compensation. It is confirmed that the current ripple has been remarkably reduced after the compensation. Thus, it can be said that the proposed method tracks the correct value of $\hat{V}_{\text{sat,DT}}$ well.

The third experiment in Fig. 15 verifies the analysis of $\delta\hat{\mathbf{v}}^{\mathbf{i}}_{\mathbf{dqs,CP,Fund}}(\phi_i)$ and $\delta\hat{\mathbf{v}}^{\mathbf{i}}_{\mathbf{dqs,DP,Fund}}(\phi_i)$ in Section IV. As shown in Fig. 15(a), i^e_{ds} and i^e_{qs} are regulated as

$$i^{e*}_{ds} = 8\cos(\phi^*), \quad i^{e*}_{qs} = 8\sin(\phi^*) \tag{25}$$

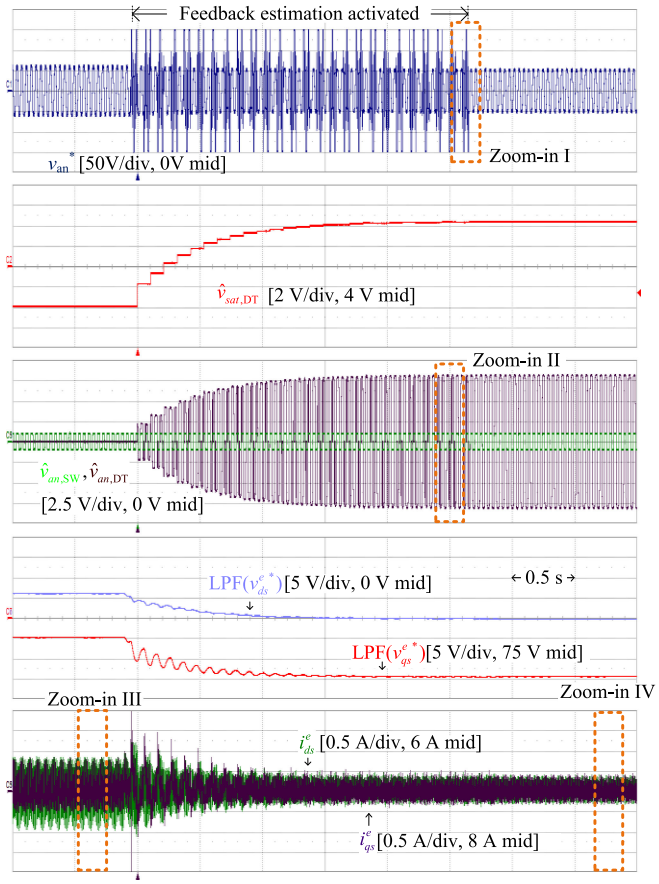

Fig. 13. Second experimental result: $\hat{V}_{\mathrm{sat,DT}}$ identification from zero initial value with the feedback method.

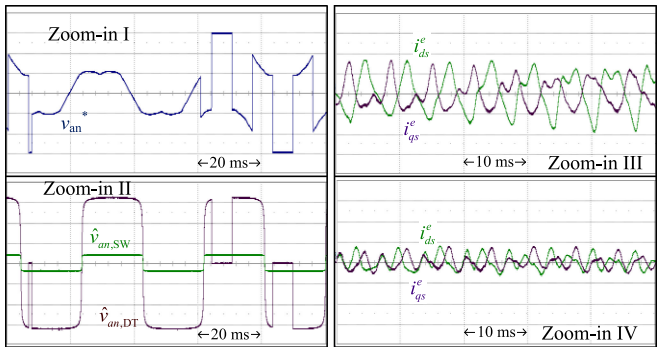

Fig. 14. Magnified view of Fig. 13.

where ϕ^* varies from -0.2π to 0.45π, and the speed is regulated as 300 r/min by the load machine. To see INE at different PWM schemes, INE compensation is not applied. Thus, even i_{ds}^e and i_{qs}^e , and speed are the same, the output of the current controller v_{ds}^{e*} and v_{qs}^{e*} are different, as shown in the second trace of Fig. 15(a). Meanwhile, $\delta\hat{\mathbf{v}}^{\mathbf{i}}_{\mathbf{dqs,CP,Fund}}(\phi_i)$ and $\delta\hat{\mathbf{v}}^{\mathbf{i}}_{\mathbf{dqs,DP,Fund}}(\phi_i)$ are unable to be measured directly, so the difference between them is achieved as

$$\delta\hat{\mathbf{v}}^{\mathbf{i}}_{\mathbf{dqs,CP,Fund}}(\phi_i) - \delta\hat{\mathbf{v}}^{\mathbf{i}}_{\mathbf{dqs,DP,Fund}}(\phi_i) = \mathrm{LPF}(\mathbf{v}^{\mathbf{i}*}_{\mathbf{dqs,CP}}) - \mathrm{LPF}(\mathbf{v}^{\mathbf{i}*}_{\mathbf{dqs,DP}}) \quad (26)$$

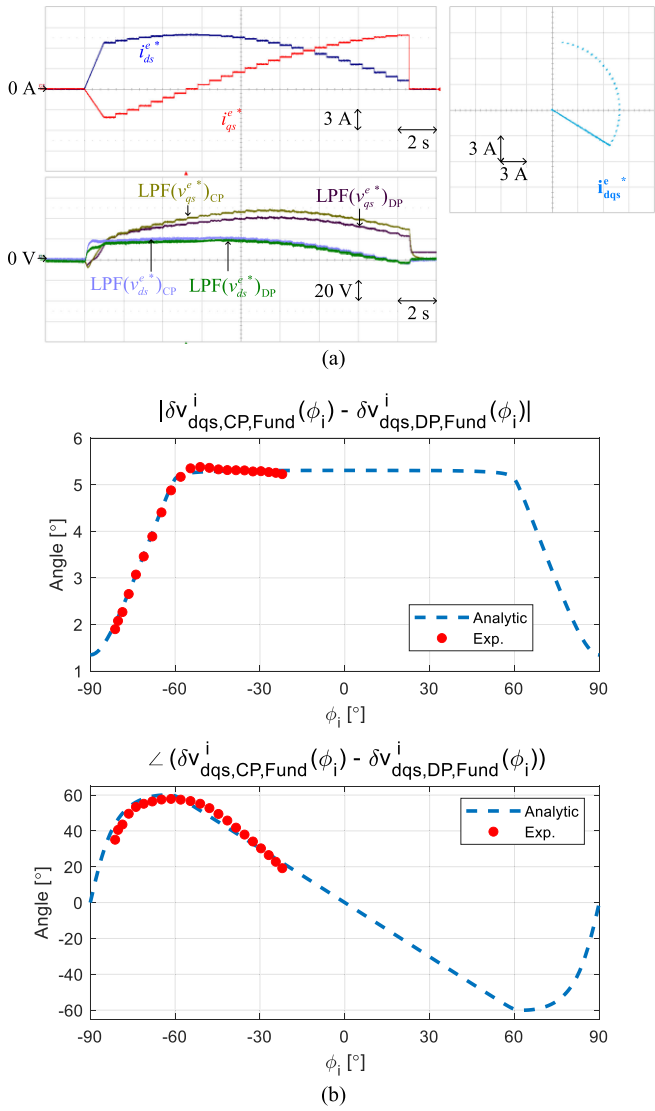

Fig. 15. Third experimental result. (a) Current and voltage reference with different PWM schemes. (b) Difference between $\delta\hat{\mathbf{v}}^{\mathbf{i}}_{\mathbf{dqs,CP,Fund}}(\phi_i)$ and $\delta\hat{\mathbf{v}}^{\mathbf{i}}_{\mathbf{dqs,DP,Fund}}(\phi_i)$: comparison of the analytic solution and experimental result.

where x is the CP or DP. Here, ϕ_i is calculated from (24). Fig. 15(b) shows the result, and the magnitude and phase of the difference in (26). While the analytic result is expressed in the entire ϕ_i from $-90°$ to $90°$, the experimental result is only from $-80°$ to $-25°$ because of the practical operating points of IM. Thus, it is confirmed that the analytic derivation for the feedforward method is well agreed with the experimental result.

Fig. 16 shows the fourth experiment that confirms the performance of the proposed feedforward-based $\hat{V}_{\mathrm{sat,DT}}$ identification when the initial value of $\hat{V}_{\mathrm{sat,DT}}$ is set to zero. The current and speed conditions are the same as those in the first and second experiments. As shown in the first and second trace, only after one alternation between CPWM and DPWM for 170 ms, $\hat{V}_{\mathrm{sat,DT}}$ reaches 8.3 V. Also, comparing Zoom-in I and II in the last trace, the current ripple is reduced by 50% same as the second

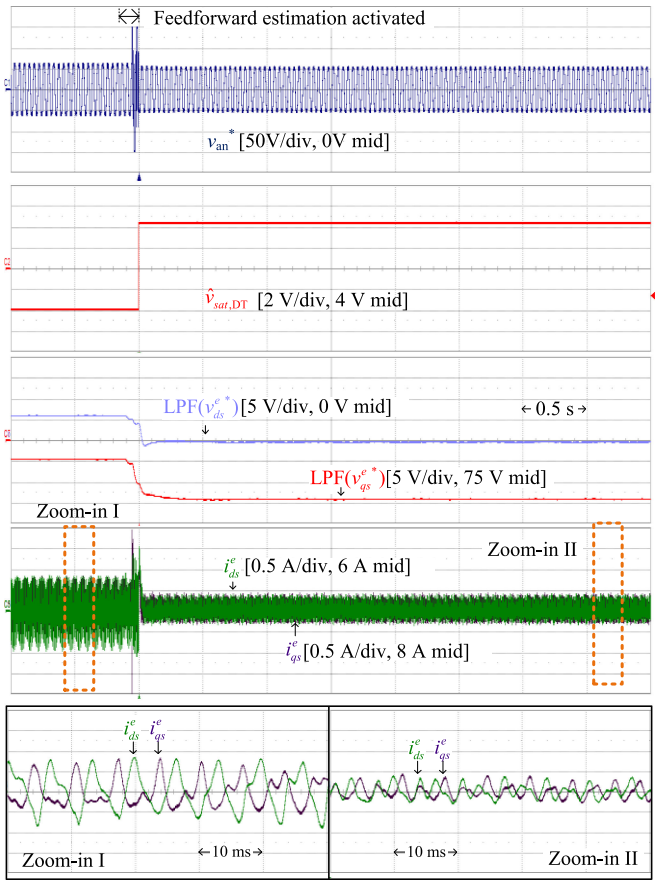

Fig. 16. Fourth experimental result: $\hat{V}_{\mathrm{sat,DT}}$ identification from zero initial value with the feedforward method.

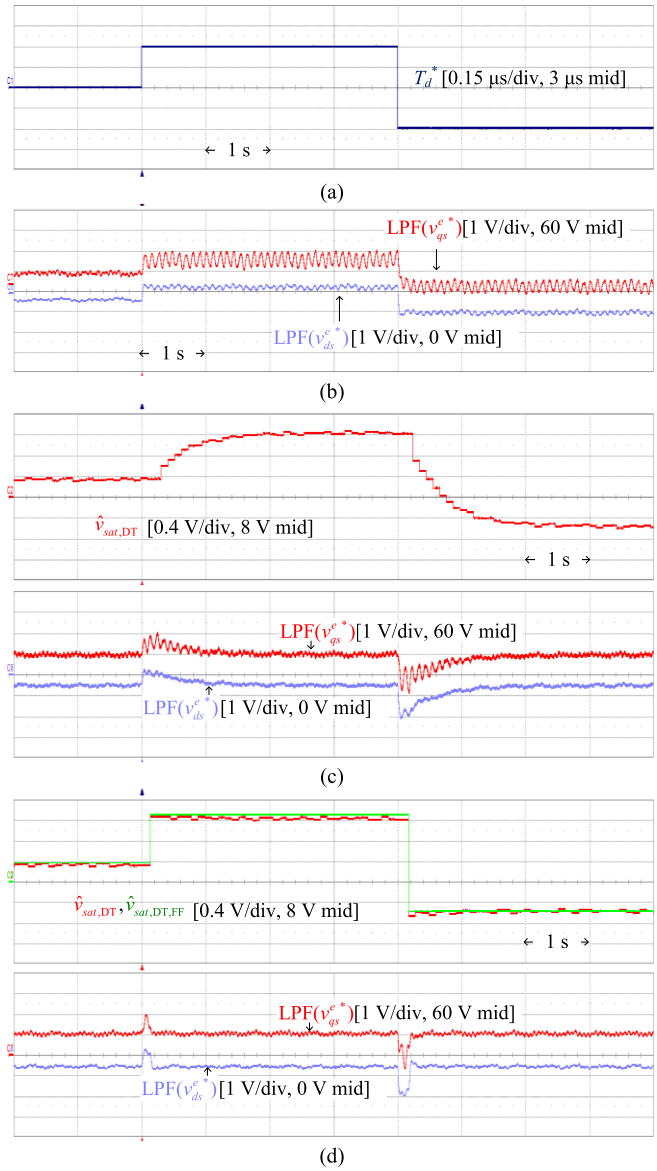

Fig. 17. Fifth experimental result. (a) $T_d{}^*$ variation. (b) $\mathrm{LPF}(v_{ds}^{e*})$ and $\mathrm{LPF}(v_{ds}^{e*})$ without the proposed method (constant $\hat{V}_{\mathrm{sat,DT}}$). (c) $\hat{V}_{\mathrm{sat,DT}}$, $\mathrm{LPF}(v_{ds}^{e*})$, and $\mathrm{LPF}(v_{ds}^{e*})$ with the feedback method. (d) $\hat{V}_{\mathrm{sat,DT}}$, $\mathrm{LPF}(v_{ds}^{e*})$, and $\mathrm{LPF}(v_{ds}^{e*})$ with the feedforward method.

experiment. Compared with the feedback-based method, the identification becomes 16.6 times faster.

The fifth experiment is shown in Fig. 17. In this experiment, T_d^* changes intentionally from 3 to 3.3 and 2.7 μs to test $\hat{V}_{\mathrm{sat,DT}}$ tracking performance, as shown in Fig. 17(a). Fig. 17(b) depicts the case when the proposed identification is not activated, so $\hat{V}_{\mathrm{sat,DT}}$ stays at the initial value, 8.3 V. Since the variation of T_d^* results in that of the disturbance voltage due to the deadtime effect, v_{ds}^{e*} and v_{qs}^{e*} are fluctuating with different PWM schemes. Also, the dc component becomes different because of T_d variation. Meanwhile, Fig. 17(b) shows that the proposed feedback-based method adjusts $\hat{V}_{\mathrm{sat,DT}}$, and it converges to 9.2 and 7.5 V, when T_d^* changes to 3.3 and 2.7 μs, respectively. The convergence points are less by about 1 V compared with the saturated value in the result of the pretest in Fig. 11(b). This is because the saturated values in Fig. 11(b) contain not only $\hat{V}_{\mathrm{sat,DT}}$ but also $\hat{V}_{\mathrm{sat,SW}}$, 1 V. Thus, the result of the proposed method is well matched with the result of the pretest. Also, the steady-state value of v_{ds}^{e*} and v_{qs}^{e*} is the same even in T_d^* because INE is well compensated by the proposed method and v_{ds}^{e*} and v_{qs}^{e*} only contain the voltage for the current control. Fig. 17(c) depicts the case when the proposed feedforward-based method is applied. Compared with Fig. 17(b), the dynamic performance becomes much faster, so the transient response time in v_{ds}^{e*} and that in v_{qs}^{e*} are remarkably reduced. Therefore, it can be said that the proposed method well tracks $\hat{V}_{\mathrm{sat,DT}}$ dynamically and accurately, even when $T_{d,\mathrm{eff}}$ changes due to the operating conditions.

Fig. 18 shows the sixth experimental result with the proposed feedback-based method in various modulation index (MI) conditions. In order to change MI, the speed of the motor changes from 1300 to 100 r/min by 400 r/min by load machine. The currents i_{ds}^e and i_{qs}^e are regulated as rated values, 6 A and 8 A. By doing so, MI changes from 0.62 to 0.09, as shown in the first trace, which is defined as

$$\mathrm{MI} = \frac{|v_{as}{}^*|}{V_{\mathrm{dc}}/\sqrt{3}}. \tag{27}$$

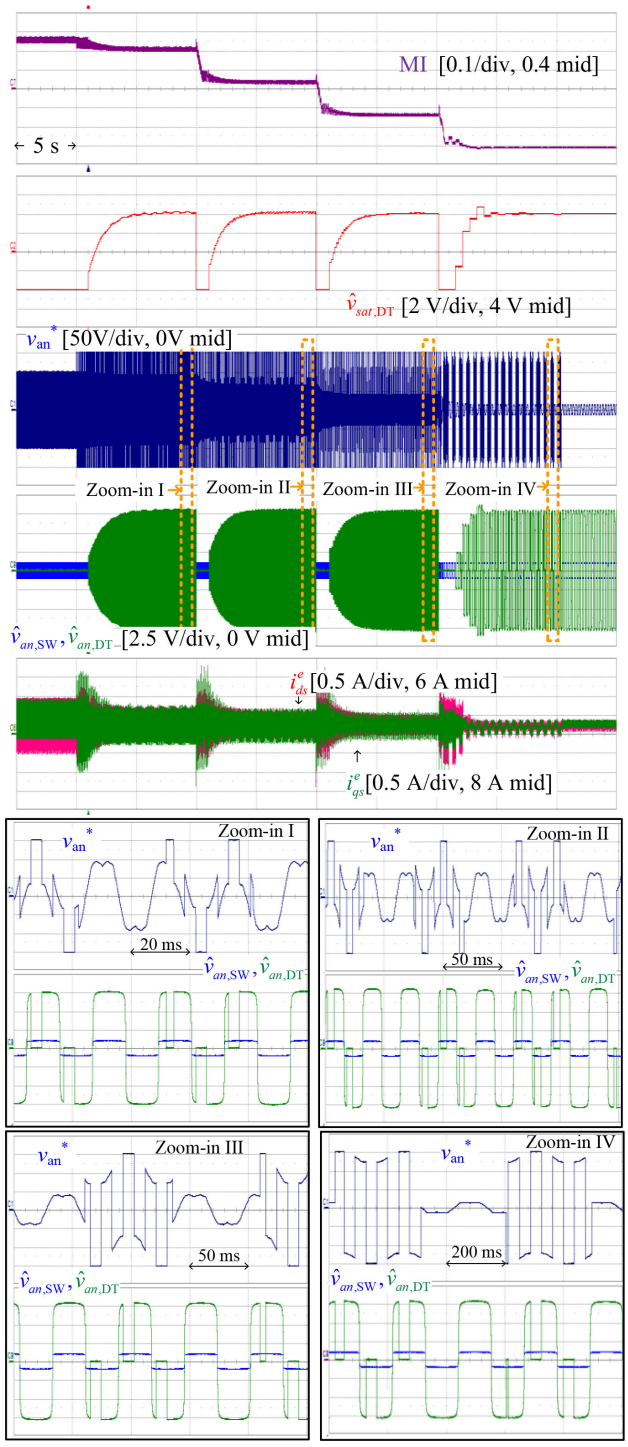

Fig. 18. Sixth experimental result: $\hat{V}_{\mathrm{sat,DT}}$ identification at various MIs with the feedback method.

The second trace shows $\hat{V}_{\mathrm{sat,DT}}$. To examine the performance of the proposed method, $\hat{V}_{\mathrm{sat,DT}}$ is reset to zero for 1 s, when the speed changes. Unlike the other cases, there is an overshoot in $\hat{V}_{\mathrm{sat,DT}}$ when MI is 0.09 because the amount of error in one sampling is quite larger compared with the other cases. However, the steady-state values of $\hat{V}_{\mathrm{sat,DT}}$ converge from 8.1 to 8.2 V in all MI conditions. Therefore, it can be said that the proposed method is effective in various MI conditions, even when the MI is at 0.09.

VI. Conclusion

This article describes the inverter nonlinearity compensation by identifying the variation of the deadtime effect according to operating conditions and manufacturing tolerance. It is based on that the deadtime effect varies with the PWM scheme. With the current controller and alternation of PWM schemes, the information of the deadtime effect can be extracted online. Also, the deadtime effect with different PWM schemes is analytically formulated. Based on that the feedforward identification method has been proposed to improve the dynamic performance. The experimental results have revealed that the identification time decreases down to 0.15 s. In addition, the resolution of the voltage error due to the deadtime effect identified by the proposed method is 100 mV range, and it is equivalent to 30 ns variation of $T_{d,\mathrm{eff}}$ in the case of 300 V dc-link voltage of the inverter.

References

[1] P. L. Jansen and R. D. Lorenz, "Transducerless position and velocity estimation in induction and salient AC machines," *IEEE Trans. Ind. Appl.*, vol. 31, no. 2, pp. 240–247, Mar./Apr. 1995.

[2] M. W. Degner and R. D. Lorenz, "Using multiple saliencies for the estimation of flux, position, and velocity in AC machines," *IEEE Trans. Ind. Appl.*, vol. 34, no. 5, pp. 1097–1104, Sep./Oct. 1998.

[3] K. Liu and Z. Q. Zhu, "Online estimation of the rotor flux linkage and voltage-source inverter nonlinearity in permanent magnet synchronous machine drives," *IEEE Trans. Power Electron.*, vol. 29, no. 1, pp. 418–427, Jan. 2014.

[4] I. Boldea, M.-C. Paicu, and G.-D. Andreescu, "Active flux concept for motion-sensorless unified AC drives," *IEEE Trans. Power Electron.*, vol. 23, no. 5, pp. 2612–2618, Sep. 2008.

[5] G. Wang, H. Zhan, G. Zhang, X. Gui, and D. Xu, "Adaptive compensation method of position estimation harmonic error for EMF-based observer in sensorless IPMSM drives," *IEEE Trans. Power Electron.*, vol. 29, no. 6, pp. 3055–3064, Jun. 2014.

[6] A. Guha and G. Narayanan, "Impact of undercompensation and overcompensation of dead-time effect on small-signal stability of induction motor drive," *IEEE Trans. Ind. Appl.*, vol. 54, no. 6, pp. 6027–6041, Nov./Dec. 2018.

[7] D. Leggate and R. J. Kerkman, "Pulse-based dead-time compensator for PWM voltage inverters," *IEEE Trans. Ind. Electron.*, vol. 44, no. 2, pp. 191–197, Apr. 1997.

[8] J. S. Kim, J. W. Choi, and S.-K. Sul, "Analysis and compensation of voltage distortion by zero current clamping in voltage-fed PWM inverter," in *Proc. Int. Power Electron. Conf.*, Apr. 3–7, 1995, pp. 265–270.

[9] Z. Zhang and L. Xu, "Dead-time compensation of inverters considering snubber and parasitic capacitance," *IEEE Trans. Power Electron.*, vol. 29, no. 6, pp. 3179–3187, Jun. 2014.

[10] N. Bedetti, S. Calligaro, and R. Petrella, "Self-commissioning of inverter dead-time compensation by multiple linear regression based on a physical model," *IEEE Trans. Ind. Appl.*, vol. 51, no. 5, pp. 3954–3964, Sep./Oct. 2015.

[11] T. Mannen and H. Fujita, "Dead-time compensation method based on current ripple estimation," *IEEE Trans. Power Electron.*, vol. 30, no. 7, pp. 4016–4024, Jul. 2015.

[12] Y. Park and S.-K. Sul, "A novel method utilizing trapezoidal voltage to compensate for inverter nonlinearity," *IEEE Trans. Power Electron.*, vol. 27, no. 12, pp. 4837–4846, Dec. 2012.

[13] G. Pellegrino, R. I. Bojoi, P. Guglielmi, and F. Cupertino, "Accurate inverter error compensation and related self-commissioning scheme in sensorless induction motor drives," *IEEE Trans. Ind. Appl.*, vol. 46, no. 5, pp. 1970–1978, Sep./Oct. 2010.

[14] H.-S. Kim, H.-T. Moon, and M.-J. Youn, "On-line dead-time compensation method using disturbance observer," *IEEE Trans. Power Electron.*, vol. 18, no. 6, pp. 1336–1345, Nov. 2003.
[15] S.-Y. Kim, W. Lee, M.-S. Rho, and S.-Y. Park, "Effective dead-time compensation using a simple vectorial disturbance estimator in PMSM drives," *IEEE Trans. Ind. Electron.*, vol. 57, no. 5, pp. 1609–1614, May 2010.
[16] T. Hoshino, J.-I. Itoh, and T. Kaneko, "Dead-time voltage error correction with parallel disturbance observers for high performance V/f control," in *Proc. IEEE Ind. Appl. Annu. Meeting*, 2007, pp. 2038–2044.
[17] J. H. Lee and S.-K. Sul, "Compensation of nonlinearity of inverter through estimation of dead time effect," in *Proc. IEEE Int. Power Electron. Motion Control Conf.*, 2020, pp. 572–577.
[18] G. Zhao, S. Nalakath, Y. Sun, J. Wiseman, and A. Emadi, "Inverter voltage drop characterisation considering junction temperature effects," in *Proc. IEEE Transp. Electrific. Conf. Expo.*, Jun. 2019, pp. 1–6.
[19] A. Guha and G. Narayanan, "Small-signal stability analysis of an open-loop induction motor drive including the effect of inverter deadtime," *IEEE Trans. Ind. Appl.*, vol. 52, no. 1, pp. 242–253, Jan./Feb. 2016.
[20] S. Ahmed, Z. Shen, P. Mattavelli, D. Boroyevich, and K. J. Karimi, "Small-signal model of voltage source inverter (VSI) and voltage source converter (VSC) considering the deadtime effect and space vector modulation types," *IEEE Trans. Power Electron.*, vol. 32, no. 6, pp. 4145–4156, Jun. 2017.
[21] Texas Instrum., Dallas, TX, USA, " ISO5852S high-CMTI 2.5-A and 5-A reinforced isolated IGBT, MOSFET gate driver with split outputs and active protection features," ISO5852S datasheet, Aug. 2015.

Joon-Hee Lee (Student Member, IEEE) was born in South Korea in 1990. He received the B.S. and Ph.D. degrees in electrical engineering from Seoul National University, Seoul, South Korea, in 2015 and 2021, respectively.

His current research interests include control of inverter, interior permanent magnet synchronous motor and induction motor (IM) drive, finite-element analysis of IM, and high-fidelity simulation of IM.

Seung-Ki Sul (Fellow, IEEE) received the B.S., M.S., and Ph.D. degrees in electrical engineering from Seoul National University, Seoul, South Korea, in 1980, 1983, and 1986, respectively.

From 1986 to 1988, he was an Associate Researcher with the Department of Electrical and Computer Engineering, University of Wisconsin, Madison, WI, USA, and from 1988 to 1990, he was a Principal Research Engineer with LG Industrial Systems Company, South Korea. Since 1991, he has been a member of Faculty with the School of Electrical and Computer Engineering, Seoul National University, where he is currently a Professor. He has authored or coauthored more than 150 IEEE journal papers and a total of more than 340 international conference papers in the area of power electronics. His current research interests include position sensorless control of electrical machines, electric/hybrid vehicles and ship drives, and power-converter circuits based on SiC MOSFET.

Dr. Sul was the Program Chair of IEEE Power Electronics Specialists Conference in 2006 and the General Chair of IEEE International Conference on Power Electronics and ECCE-Asia in 2011. From 2011 to 2014, he was the Editor-in-Chief for the *Journal of Power Electronics*, which is an SCIE-registered journal, published by the Korean Institute of Power Electronics (KIPE), Seoul, South Korea. In 2015, he was the President of KIPE. He was the recipient of the 2015 IEEE Transaction 1st and 2nd Paper Awards on Industrial Application, simultaneously, the 2016 Outstanding Achievement Award of the IEEE Industrial Application Society, and also selected for 2017 Newell Award sponsored by IEEE Power Electronics Society.